# mSAM: Micro-Batch-Averaged Sharpness-Aware Minimization

Kayhan Behdin\*<sup>1,2</sup>, Qingquan Song<sup>1</sup>, Aman Gupta<sup>1</sup>, Ayan Acharya<sup>1</sup>, David Durfee<sup>1</sup>, Borja Ocejo<sup>1</sup>, Sathiya Keerthi<sup>1</sup>, and Rahul Mazumder<sup>1,2</sup>

<sup>1</sup>LinkedIn Corporation, USA <sup>2</sup>Massachusetts Institute of Technology, USA

#### Abstract

Modern deep learning models are over-parameterized, where different optima can result in widely varying generalization performance. To account for this, Sharpness-Aware Minimization (SAM) modifies the underlying loss function to guide descent methods towards flatter minima, which arguably have better generalization abilities. In this paper, we focus on a variant of SAM known as micro-batch SAM (mSAM), which, during training, averages the updates generated by adversarial perturbations across several disjoint shards (micro batches) of a mini-batch. We extend a recently developed and well-studied general framework for flatness analysis to show that distributed gradient computation for sharpness-aware minimization theoretically achieves even flatter minima. In order to support this theoretical superiority, we provide a thorough empirical evaluation on a variety of image classification and natural language processing tasks. We also show that contrary to previous work, mSAM can be implemented in a flexible and parallelizable manner without significantly increasing computational costs. Our practical implementation of mSAM yields superior generalization performance across a wide range of tasks compared to SAM, further supporting our theoretical framework.

### 1 Introduction

Overparameterized deep neural networks (DNNs) have become a staple of modern machine learning advancements, yielding strong state-of-the-art performance for tasks in domains like image understanding [1, 2, 3], natural language processing (NLP) [4, 5, 6] and recommender systems [7, 8]. Training DNNs requires minimizing complex and non-convex loss functions with an abundance of minima. Interestingly, different minima can have varying generalizability on unseen data [9, 10]. Thus, choosing an optimization setup that can seek out minima yielding strong generalisation performance is critically important. A wide range of optimization algorithms has been developed for various domains, e.g. stochastic gradient descent (SGD), heavy-ball momentum [11], Adam [12], LAMB [13] among others. When coupled with suitable regularization techniques, these methods help yield strong generalization performance. The ability to perform implicit regularization of SGD-like methods has thus received considerable attention in the literature in recent years [14, 15].

Recently, extensive work has been done to study the correlation between the geometry of the loss landscape and generalization performance [9, 16, 17, 18, 19, 20]. The newly proposed Sharpness-Aware Minimization (SAM) algorithm [21] leverages this correlation between the flatness of minima and generalization performance by modifying the loss function to seek flatter solutions during training, leading to superior generalization for a panoply of tasks and domains. In particular, this method changes the loss function to consider the maximum value in a small neighbourhood around the current parameters in the loss landscape. The gradient descent step for this loss function is achieved by performing the composition of two steps, the first being an

<sup>\*</sup>behdin1675@gmail.com

adversarial perturbation. Intuitively, SAM represents flatness by looking at the gradients in one particular adversarial direction to descend according to the worst-case sharpness.

Unlike standard gradient descent (GD), the compositional nature of the SAM gradient computation implies that further splitting the mini-batch into disjoint shards (micro-batches) and averaging the updates will not lead to the same gradient. This was noted in Foret et al. [21], where they introduced this notion as mSAM, with m being the number of micro-batches of a single mini-batch. By splitting into disjoint shards, mSAM leverages several adversarial directions, which may more robustly represent flatness. In this work, we build the corresponding theoretical framework for improved flatness of mSAM that utilizes and extends previous techniques. Our extensive experimental results confirm these insights on a wide range of tasks. While the focus will particularly be on mSAM, our techniques apply more generally. They further imply that splitting the mini-batch for compositional gradient computations, utilized in other variants of SAM, may also lead to an improved flatness of minima. Such observations invariably encourage further study of splitting the mini-batch into shards whenever the gradient update follows a non-linear aggregation.

Related Work: Although the sharpness of the loss landscape can be calculated using several different measures (for example, the largest eigenvalue [22] or trace [23] of the Hessian of the loss), most of these measures are computationally too expensive for practical purposes. Since it has been shown that the sharpness of the loss landscape correlates with generalization [9], the main idea behind the SAM [21] algorithm is to encourage the network to seek regions where the worst loss value in a local neighbourhood is not too large (see Section 2 for more details). This proxy of sharpness lends itself to easy computation, unlike the measures of sharpness described earlier. SAM has sparked interest in sharpness-aware training, resulting in several variants [24, 25, 26, 27, 28].

In this paper, we focus on the effect of further splitting the mini-batch into shards for gradient computation of sharpness-aware minimization methods. While our theoretical results on flatness will generalize, we primarily consider mSAM, which is this technique applied to the original SAM algorithm. In [21], mSAM is used *implicitly* to reduce the computational cost of SAM by avoiding synchronization across multiple GPUs (referred to as "accelerators" hereinafter). Recently, it has been observed via limited experimentation that mSAM results in better generalization performance [21, 29, 30]. The authors of [31] present mathematical expressions for mSAM, but their analysis is primarily focused on a particular version of mSAM (see Section 2 for more details). The experiments are also limited to image classification tasks on small architectures. This paper provides a more general theoretical framework that can also be extended to other sharpness-aware minimization variants.

Several recent papers on the stability analysis of gradient descent (GD) and SGD-like algorithms reveal that these methods operate on the edge of stability [14, 15, 32, 33], where the maximum eigenvalue of the training loss Hessian hovers around the value  $2/\eta$ ,  $\eta$  being the learning rate. These results can then be leveraged to devise upper bounds on the maximum eigenvalue of the training loss Hessian (see Section 3 for more details).

Our Contributions: Our contributions in this paper can be summarized as follows:

- We demonstrate how mSAM improves flatness over SAM, which in turn guarantees better flatness than SGD. To that end, we leverage theoretical ideas about the implicit generalization ability of SGD-like methods and recent work related to the stability analysis of full-batch GD and SGD.
- Starting from the mathematical description of mSAM, we present an *explicit* and flexible implementation of mSAM that does not rely on accelerator synchronization and is compatible with any single/multi-accelerator setup.
- We conduct extensive experiments on a wide variety of tasks for computer vision and natural language processing, leveraging architectures like Convolutional Neural Networks (CNNs) [1, 2] and Transformers [4], where mSAM consistently outperforms SAM and vanilla training.

### 2 Algorithm

In this section, we rigorously introduce mSAM, based on the SAM algorithm that aims to obtain flat solutions to the empirical loss function. In particular, SAM tries to find a solution that minimizes the worst-case loss in a ball around the solution. Mathematically, let  $\mathcal{S} = \{(\mathbf{x}_i, y_i), i \in [n] : \mathbf{x}_i \in \mathcal{X}, y_i \in \mathcal{Y}\}$  be a dataset of n samples, where  $\mathcal{X}$  is the set of features and  $\mathcal{Y}$  is the set of outcomes. Moreover, let  $\ell : \mathbb{R}^d \times \mathcal{X} \times \mathcal{Y} \mapsto \mathbb{R}$  be a differentiable loss function, where d is the number of model parameters. The empirical loss over the dataset  $\mathcal{S}$  is defined as  $\mathcal{L}_{\mathcal{S}}(\mathbf{w}) = \sum_{i=1}^{n} \ell(\mathbf{w}; \mathbf{x}_i, y_i)/n$ , where w parameterizes the neural network. With this notation in place, the SAM loss function is defined as [21]:

$$\mathcal{L}_{\mathcal{S}}^{SAM}(\mathbf{w}) = \max_{\|\epsilon\|_{\infty} < \rho} \mathcal{L}_{\mathcal{S}}(\mathbf{w} + \epsilon)$$
(1)

for some  $p \ge 1$ . In this work, we use p = 2. In practice, however, the maximization step in (1) cannot be done in closed form. Hence, authors in [21] use a first-order approximation to  $\mathcal{L}_S$  to simplify (1) as

$$\mathcal{L}_{\mathcal{S}}^{SAM}(\mathbf{w}) \approx \max_{\|\epsilon\|_{2} \leq \rho} \mathcal{L}_{\mathcal{S}}(\mathbf{w}) + \epsilon^{T} \nabla \mathcal{L}_{S}(\mathbf{w}). \tag{2}$$

It is easy to see that the maximum in Problem (2) is achieved for

$$\hat{\epsilon} = \rho \nabla \mathcal{L}_{\mathcal{S}}(\mathbf{w}) / \| \nabla \mathcal{L}_{\mathcal{S}}(\mathbf{w}) \|_{2}. \tag{3}$$

As a result,  $\mathcal{L}_{\mathcal{S}}^{SAM} \approx \mathcal{L}_{\mathcal{S}}(w + \hat{\epsilon})$ . This leads to the gradient

$$\nabla \mathcal{L}_{\mathcal{S}}^{SAM}(\mathbf{w}) \approx \nabla_{\mathbf{w}} \left[ \mathcal{L}_{\mathcal{S}}(\mathbf{w} + \hat{\epsilon}) \right] = \frac{\partial (\mathbf{w} + \hat{\epsilon})}{\partial \mathbf{w}} \nabla \mathcal{L}_{\mathcal{S}}(\mathbf{w} + \hat{\epsilon}).$$

However, calculating  $\partial(w+\hat{\epsilon})/\partial w$  involves second-order terms that require access to Hessian, which can be computationally inefficient in practice. Thus, by ignoring the second-order terms in the above approximation, the gradient of the SAM loss can be approximated as [21]:

$$\nabla \mathcal{L}_{\mathcal{S}}^{SAM}(\mathbf{w}) \approx \nabla \mathcal{L}_{\mathcal{S}}(\mathbf{w} + \rho \nabla \mathcal{L}_{\mathcal{S}}(\mathbf{w}) / \|\nabla \mathcal{L}_{\mathcal{S}}(\mathbf{w})\|_{2})$$
(4)

which is used in the SAM algorithm (for example, in conjunction with SGD). We refer to [21] for more details and intuitions about SAM. We call the inner gradient calculations on the right-hand side of (4) as the SAM ascent step and the outer gradient calculations as the gradient step. mSAM [21] is a variation of the SAM algorithm. In general, for mSAM, a mini-batch of data  $\mathcal{S}$  is further divided into m smaller disjoint shards (aka "micro-batches"), such as  $\mathcal{S}_1, \dots, \mathcal{S}_m$  where  $\bigcup_{i=1}^m \mathcal{S}_i = \mathcal{S}$ . For simplicity, we assume  $|\mathcal{S}_1| = \dots = |\mathcal{S}_m| = |\mathcal{S}|/m$  although such an assumption is not necessary in general. The mSAM loss is a variation of the SAM loss, defined as:

$$\mathcal{L}_{\mathcal{S}}^{mSAM}(\mathbf{w}) = \frac{1}{m} \sum_{i=1}^{m} \max_{\|\epsilon^{(i)}\|_{2} \le \rho} \mathcal{L}_{\mathcal{S}_{i}}(\mathbf{w} + \epsilon^{(i)}).$$
 (5)

Intuitively, mSAM is a version of SAM where the ascent step (or the weight perturbation) of SAM is done independently on each micro-batch using different  $\epsilon^{(i)}$ , instead of using an average perturbation such as  $\epsilon$  for all micro-batches. The mSAM gradient can thereby be derived as:

$$\nabla \mathcal{L}_{\mathcal{S}}^{mSAM}(\mathbf{w}) = \frac{1}{m} \sum_{i=1}^{m} \nabla \mathcal{L}_{\mathcal{S}_i}(\mathbf{w} + \rho \nabla \mathcal{L}_{\mathcal{S}_i}(\mathbf{w}) / \|\nabla \mathcal{L}_{\mathcal{S}_i}(\mathbf{w})\|_2), \tag{6}$$

where (6) is a first-order approximation to the gradient of (5). We also note that the loss (5) is related to the mSAM definition of [31]. See Table 1 for a side-by-side comparison of SAM and mSAM and their different implementations.

An important distinction between our work and prior work is that we treat m as a model hyper-parameter to improve generalization. In particular, in mSAM implementation of [21], the value of m is fixed to the

Table 1: Comparison of SAM with Different mSAM Implementations. [FKMN] refers to Foret et al. [21] and [AF] refers to Andriushchenko and Flammarion [31].

	SAM		мSAM			
Loss function	$\max_{\ \epsilon\ _2 \le \rho} \sum_{i=1}^m \mathcal{L}_{\mathcal{S}_i}(\mathbf{w} + \epsilon) / m \qquad \qquad \sum_{i=1}^m \max_{\ \epsilon^{(i)}\ _2 \le \rho} \mathcal{L}_{\mathcal{S}_i}(\mathbf{w} + \epsilon^{(i)}) / m$		(i)/m			
ASCENT STEP	$\hat{\epsilon} \propto \rho \sum_{i=1}^{m} \nabla \mathcal{L}_{\mathcal{S}_i}(\mathbf{w})/m$	$\hat{\epsilon}^{(i)} \propto  ho  abla \mathcal{L}_{\mathcal{S}_i}(\mathbf{w}), \ i \in [m]$		n]		
Gradient	$g = \sum_{i=1}^{m} \nabla \mathcal{L}_{\mathcal{S}_i}(\mathbf{w} + \hat{\epsilon})/m$	$g = \sum_{i=1}^{m} \nabla \mathcal{L}_{\mathcal{S}_i}(\mathbf{w} + \hat{\epsilon}^{(i)})/m$		/m		
Implementations	[FKMN]	[FKMN] [AF] Out		Ours		
Possible $m$ values	-	# OF ACCELERATORS FLEXIB		FLEXIBLE		
PROCESSOR SUPPORT	MULTIPLE	Multiple	SINGLE	Multiple		

number of hardware accelerators, micro-batch i is the part of the data that is loaded onto accelerator i, and each accelerator uses a separate perturbation, simulating the effect of mSAM. With this implementation, m is an artefact of the hardware setup. On the other hand, the analysis of [31] mostly concerns the value  $m = |\mathcal{S}| := B$  where  $\mathcal{S}$  is the mini-batch under consideration, and we denote its size as B for ease of use in latter sections. In contrast, we consider a wide range of values for m in our experiments—this offers the flexibility to choose an appropriate value of m that leads to a better generalization performance. Moreover, our implementation supports any single/multi-accelerator setup and allows the user to set an appropriate value of m.

### 3 Justification of mSAM

Over-parameterized DNNs have a continuum (a manifold of large size) of minima,  $\mathcal{M}$  due to the number of parameters being much larger than the number of training examples. An intriguing property of DNNs is that different minima in  $\mathcal{M}$  have different sharpness values. When trained using SGD with a large learning rate and small batch size, these DNNs have an implicit ability to move towards minima which are flat - or equivalently, less sharp, with sharpness expressed as the spectral norm of the Hessian<sup>1</sup> [18, 22]. Jastrzebski et al. [14], Cohen et al. [15] established a theoretical framework to explain this phenomenon with strong empirical backing. Accordingly, this approach is followed by most recent theoretical papers on analyzing the properties of GD, SGD, and SAM [15, 32, 34, 35, 36]. In this section, we review a generalized version of such analyses in Section 3.1 and extend it to SAM and mSAM in Section 3.2. This well-studied framework implies that mSAM improves flatness even further than SAM.

#### 3.1 Stability Analysis

Thanks to the rigorous theoretical and empirical analyses by Cohen et al. [15, 32], Arora et al. [33], GD on neural network training is understood to reach and operate in a regime known as the *Edge of Stability*, where the maximum eigenvalue of the training loss Hessian hovers just above the value  $2/\eta$ , where  $\eta$  is the learning rate. After reaching the *Edge of Stability* region, the training loss behaves non-monotonically over short timescales, and yet it consistently decreases over long timescales. All such theoretical findings are due to the seminal discovery by Jastrzebski et al. [14], who first performed methodical experiments to identify a similar behaviour with SGD.

In applications with over-parameterized models, all global minima are fixed points of the dynamics, but their stability properties vary. At unstable minima, a small perturbation forces the dynamics to diverge. On the other hand, for stable minima, the dynamics can converge even after initial perturbations. In particular, Wu et al. [18], Ma and Ying [37] analyze the linear stability [38] of SGD, showing that a linearly stable minimum must be flat, assuming a quadratic approximation of the loss function near the minimum. Unlike

<sup>&</sup>lt;sup>1</sup>Sharpness can also be quantified in other ways. See [14, 18, 22, 32] for some details.

analyses based on stochastic differential equations [39, 40, 41, 42, 43, 44, 45], this stability-based analysis is relevant for large learning rates and is even empirically accurate in predicting the properties of minima selected by SGD [14, 15, 18].

We first define the model dynamics that will be used for the stability analysis. Consider a DNN setup with general training dynamics defined by a descent direction,  $d(\mathbf{w}; \mathcal{H})$  that is a function of  $\mathbf{w}$ , the weight vector and  $\mathcal{H}$ , a set of hyper-parameters.  $\mathcal{H}$  includes the learning rate  $\eta$  (for simplicity, we assume a single value is used throughout the training); mini-batch size B; the training method itself, for example, (full batch) GD, SGD, SAM, mSAM; and, method-dependent hyper-parameters such as  $\rho$  (for SAM and mSAM) and the micro-batch size, b = B/m (for mSAM). The dynamics can be defined as:

$$\mathbf{w}_{(t+1)} = \mathbf{w}_t - d(\mathbf{w}_t; \mathcal{H}) \tag{7}$$

Note that the system is deterministic when B equals n, the number of training examples. The system turns stochastic when the mini-batch is chosen randomly at each update step.

Since all training methods aim to minimise the total training loss, the continuum of minima,  $\mathcal{M}$  can also be assumed to be the set of equilibrium points of the dynamic system (7) for all methods. Let  $\mathbf{w}^*$  represent a generic minimum in that continuum. Expectedly, the stability properties of the trajectories around  $\mathbf{w}^*$  depend on  $\mathcal{H}$ .

#### 3.1.1 Flatness of GD

For GD, the edge of stability condition corresponds to the following:

$$\lambda_{\text{max}}(\mathbf{I} - \eta \mathbf{H})^2 = 1,\tag{8}$$

where  $\mathbf{H} = \frac{1}{n} \sum_{i} \mathbf{H}_{i}$  is the Hessian of the full batch loss,  $\mathbf{H}_{i}$  is the Hessian of the loss due to the *i*-th example, and  $\lambda_{\max}(\mathbf{X})$  denotes the largest eigenvalue of matrix  $\mathbf{X}$ .

One can see that the above dynamical system diverges as soon as we have  $(1 - \eta \lambda) > -1$  even for one eigenvalue of  $\mathbf{H}$ ,  $\lambda$ . Therefore, the dynamics achieves stable equilibrium only when  $\eta \leq \frac{2}{\lambda}$  for all eigenvalues. In other words, for the dynamics of the gradient descent to converge, we must have

$$\eta \le \frac{2}{\lambda_{\max}(\mathbf{H})} \stackrel{\text{def}}{=} \hat{\eta}_{GD}.$$
(9)

Note that a larger  $\lambda_{\max}(\mathbf{H})$  imposes a tighter bound on the learning rate. Said differently, given  $\lambda_{\max}(\mathbf{H})$ , a large learning rate value causes the GD dynamics to diverge from the minimum. Another interpretation is that, for satisfying the stability condition (8), larger the  $\eta$ , smaller will be the sharpness  $\lambda_{\max}(\mathbf{H})$ .

### 3.1.2 Flatness of SGD

For SGD, under suitable quadratic approximations of the loss around a minimum, the edge of stability condition admits the following form [14, 22]:

$$\lambda_{\max}\left((\mathbf{I} - \eta \mathbf{H})^2 + \frac{\eta^2(n-B)}{B(n-1)}\mathbf{\Sigma}\right) = 1$$
(10)

where **H** is the full batch Hessian as defined earlier, and  $\Sigma = \text{Var}(\mathbf{H}_i) = \frac{1}{n} \sum_i \mathbf{H}_i^2 - \mathbf{H}^2$  is the covariance of the SGD noise. The above condition reduces to (8) when B = n.

Note that the components in (10) that contribute to the flatness have different physical interpretations. The first component  $(\mathbf{I} - \eta \mathbf{H})^2$  is due to the GD dynamics, and the other component  $\frac{\eta^2(n-B)}{B(n-1)}\Sigma$  comes from the stochastic mini-batches. The stability condition of (10) leads to the following constraint on  $\eta$ :

$$(1 - \eta \lambda_{\max}(\mathbf{H}))^2 + \eta^2 \frac{(n-B)}{B(n-1)} \sigma^2 \le 1$$

which leads to a limiting  $\hat{\eta}_{SGD}$  that satisfies  $\hat{\eta}_{SGD} < \hat{\eta}_{GD}$ . Here  $\sigma^2$  is the component of the noise variance projected onto  $\lambda_{\max}(\mathbf{H})$  [14]. In general, when  $\mathbf{w}^*$  satisfies (10), the close relation between  $\Sigma$  and  $\mathbf{H}$  implies that the set of hyper-parameters  $\mathcal{H}$  is crucial for determining the sharpness of the  $w^*$  reached [18]. In particular, for SGD, the larger the learning rate  $\eta$ , the lesser the sharpness of  $\mathbf{w}^*$  reached. Contrastingly, the smaller the mini-batch size B, the lesser the sharpness of  $\mathbf{w}^*$ .

### 3.2 Flatness of SAM and mSAM

Given the complexity of the dynamics involved in SAM and mSAM, the corresponding edge of stability analysis with arbitrary loss function gets complicated and we will make suitable assumptions. In line with Wu et al. [18, 22], Bartlett et al. [34], Wen et al. [35], we assume that in the neighborhood of a given minimum  $\mathbf{w}^*$ , the loss on each example i behaves quadratically as  $L_i(\mathbf{w}) \approx \frac{1}{2}(\mathbf{w} - \mathbf{w}^*)^T \mathbf{A}_i(\mathbf{w} - \mathbf{w}^*)$ . With such an assumption, note that the per-example Hessian is  $\mathbf{H}_i = \mathbf{A}_i$ . Consistent with the empirical observations (see section 4), we develop analyses that decipher that SAM reduces sharpness over GD/SGD, and mSAM further reduces sharpness over SAM. We begin by looking at the full batch version of the methods. The mini-batch version will be covered in subsubsection 3.2.2.

#### 3.2.1 Flatness of Full batch SAM and mSAM

Let  $\mathbf{A} = \mathbb{E}[\mathbf{A}_i]$ . To simplify, consider an approximation to the SAM dynamics that ignores the normalization term<sup>3</sup> associated with the ascent direction in SAM:

$$\mathbf{w}_{(t+1)} = \mathbf{w}_t - \eta \mathbf{A} (\mathbf{w}_t + \rho \mathbf{A} \mathbf{w}_t) = (\mathbf{I} - \eta \mathbf{A} - \eta \rho \mathbf{A}^2) \mathbf{w}_t.$$

The corresponding edge of stability condition can be written as:

$$\lambda_{\text{max}} \left( \mathbf{I} - \eta \mathbf{A} - \eta \rho \mathbf{A}^2 \right)^2 = 1. \tag{11}$$

Like in the case of GD or SGD, this dynamics achieves a stable state only when

$$\eta \le \frac{2}{\lambda_{\max}(\mathbf{A})(1 + \rho\lambda_{\max}(\mathbf{A}))} \stackrel{\text{def}}{=} \hat{\eta}_{SAM}.$$
(12)

Note using (8) and (11) how SAM achieves better flatness than GD because of the presence of the term with  $A^2$  in its dynamics.

For the stability analysis of mSAM, we further assume that each  $\mathbf{A}_i$  is a diagonal matrix. Let  $\tilde{\mathbf{A}}$  denote the mean of  $\mathbf{A}_i$  over a micro-batch of the mSAM dynamics. The corresponding dynamics is given by:

$$\mathbf{w}_{(t+1)} = \mathbf{w}_t - \eta \mathbb{E}[\tilde{\mathbf{A}}^T (\mathbf{w}_t + \rho^T \tilde{\mathbf{A}} \mathbf{w}_t)]$$
$$= (\mathbf{I} - \eta \mathbb{E}[\tilde{\mathbf{A}}] - \eta \rho \mathbb{E}[\tilde{\mathbf{A}}^2]) \mathbf{w}_t.$$

Let b = B/m be the micro-batch size. With  $\mathbf{A} = \mathbb{E}[\tilde{\mathbf{A}}]$  and  $\operatorname{Var}(\tilde{\mathbf{A}}) = \frac{1}{b}\operatorname{Var}(\mathbf{A}_i) = \frac{1}{b}\boldsymbol{\Sigma}$ , we arrive at the following dynamics:

$$\mathbf{w}_{(t+1)} = (\mathbf{I} - \eta \mathbf{A} - \eta \rho (\mathbf{A}^2 + \frac{1}{b} \mathbf{\Sigma})) \mathbf{w}_t.$$

The edge of stability condition for mSAM can be written as:

$$\lambda_{\max} \left( \mathbf{I} - \eta (\mathbf{A} (\mathbf{I} + \rho \mathbf{A}) + \frac{\rho}{b} \mathbf{\Sigma}) \right)^2 = 1$$
 (13)

That mSAM further reduces sharpness over SAM is clear from the presence of the  $\frac{\rho}{b}\Sigma$  term. mSAM dynamics achieves a stable state only when

$$\eta \le \frac{2}{\lambda_{\max} \left( \mathbf{A} (\mathbf{I} + \rho \mathbf{A}) + \frac{\rho}{h} \mathbf{\Sigma} \right)} \stackrel{\text{def}}{=} \hat{\eta}_{mSAM}$$
 (14)

<sup>&</sup>lt;sup>2</sup>For cross-entropy loss, this quadratic approximation assumption is sound if label smoothing [46] is applied.

<sup>&</sup>lt;sup>3</sup>Another way to look at this assumption is to use a zeroth order approximation of the normalization term.

It is easy to see from (9), (12) and (14) that

$$\hat{\eta}_{mSAM} \le \hat{\eta}_{SAM} \le \hat{\eta}_{GD} \tag{15}$$

showing that mSAM is the method that is most susceptible to instability, thereby forcing the value of sharpness needed to meet the edge-of-stability condition to be the least.

An interesting principle emerges from the stability-based discussions in this section: any method that brings an additional term to the Hessian of d(w; H) that is related to the Hessian of the loss will help decrease sharpness. This further implies that for any descent method that uses a composition of gradients, which is often seen in sharpness-aware minimization variants [24, 25], the micro-batching of the mini-batch can further improve the flatness.

#### 3.2.2 Flatness of Mini-batch SAM and mSAM

The extension of (10) to SAM and mSAM is straightforward if we note that (10) is based on the following derivation in Wu et al. [22]. For any generic stochastic mini-batch matrix  $\mathbf{X} = \frac{1}{B} \sum_{i} \mathbf{X}_{i}$  and corresponding dynamics  $\mathbf{w}_{(t+1)} = \mathbf{w}_{t} - \eta \mathbf{X} \mathbf{w}_{t}$ , Wu et al. [22] show

$$\mathbb{E}[\|\mathbf{w}_{(t+1)}\|^2] = \mathbb{E}[\mathbf{w}_t^T[(\mathbf{I} - \eta \mathbb{E}\mathbf{X}_i)^2 + \frac{\eta^2(n-B)}{B(n-1)} \text{Var}(\mathbf{X}_i)]\mathbf{w}_t],$$

and derive the associated edge-of-stability condition

$$\lambda_{\max}\left(\left(\mathbf{I} - \eta \, \mathbb{E}[\mathbf{X}_i]\right)^2 + \frac{\eta^2(n-B)}{B(n-1)} \mathrm{Var}(\mathbf{X}_i)\right) = 1. \tag{16}$$

For SAM,  $\mathbf{X}_i = \mathbf{X}_{i,SAM} \stackrel{\text{def}}{=} (\mathbf{A}_i + \rho \mathbf{A_i}^2)$ , and  $\mathbb{E}[\mathbf{X}_{i,SAM}] = (\mathbf{A} + \rho \mathbf{A}^2)$ . For mSAM,  $\mathbf{X}_i = \mathbf{X}_{i,mSAM} \stackrel{\text{def}}{=} (\mathbf{A} + \rho \mathbf{A_i}^2 + \frac{\rho}{b} \mathbf{\Sigma})$ , and  $\mathbb{E}[\mathbf{X}_{i,mSAM}] = (\mathbf{A} + \rho \mathbf{A}^2 + \frac{\rho}{b} \mathbf{\Sigma})$ .

Then, using the above and the same arguments as in subsection 3.1.2, we can show that, even in the mini-batch setting, mSAM achieves lower sharpness than SAM, and SAM achieves lower sharpness than SGD.

Since  $\Sigma$  is deterministic,  $\operatorname{Var}(\mathbf{X}_{i,SAM}) = \operatorname{Var}(\mathbf{X}_{i,mSAM})$ . Thus, mini-batch stochasticity plays an equal role for SAM and mSAM. In this regard, it is worth pointing out the work of Geiping et al. [47], who use the idea of micro-batches together with gradient norm penalization. Though the method is similar to mSAM, it is done in a full batch setting which may completely miss the gains coming from mini-batch stochasticity.<sup>4</sup> However, that method is expensive and needs several other tricks to work well. Also, it has been demonstrated only on the CIFAR-10 dataset.

Despite some counter-examples proposed in Dinh et al. [48], Kaur et al. [49], generalization (measured as test error or AUC) is empirically found to be well correlated with flatness. Hence mSAM's improved flatness also translates to improved generalization. This is verified through exhaustive experiments in section 4.

### 3.3 An Experiment with Synthetic Data

To illustrate the degrees of improvements in flatness achieved by various methods, we introduce an analytical training objective function  $f: \mathbb{R}^2 \to \mathbb{R}$  of the form:

$$f(\mathbf{w}) = (w_1^2 + 1 + \sigma^2)w_2^2.$$

We can think of  $f(\cdot)$  playing the role of the expected (generalized) loss. The loss surface with white contour is displayed in Figure 1. The sparser the contour at a region, the flatter the surface at the region. For example, whenever  $w_2 = 0$ , the objective remains zero for any  $w_1$ . However, the surface becomes sharper when  $|w_1|$  becomes larger. To simulate a machine learning setup, we assume noisy objectives that are formed as

$$f_i(\mathbf{w}) = ((w_1 - a_i)^2 + 1 + b_i)w_2^2$$

<sup>&</sup>lt;sup>4</sup>The deliberate intent of Geiping et al. [47] is to use only deterministic ideas to match the performance of mini-batch methods.

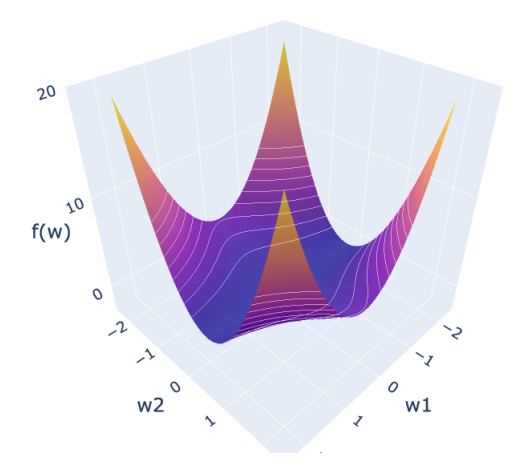


Figure 1: Surface of the synthetic objective with white contour for the  $f(\mathbf{w})$ -axis. The sparser the contour at a region, the flatter the surface at the region. For example, whenever  $w_2 = 0$ , the objective is zero  $(f(\mathbf{w}) = 0)$ , however, the surface becomes sharper when  $|w_1|$  becomes larger.

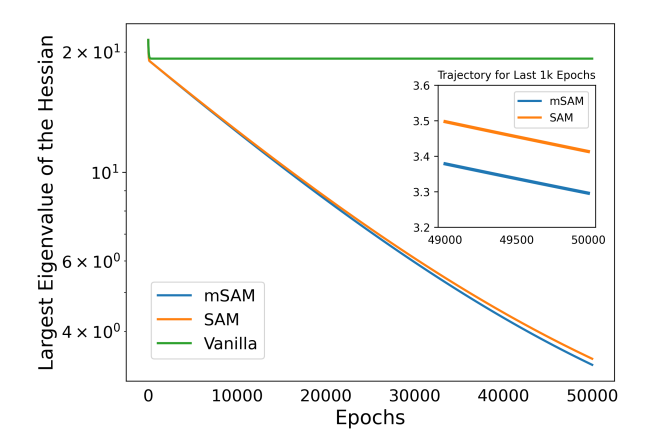


Figure 2: Trajectory of the largest eigenvalue (in logarithmic scale) of the Hessian for three methods on optimizing the synthetic data.

where  $a_i, b_i$  are independent random variables and follow the Normal distributions  $a_i \sim \mathcal{N}(0, \sigma^2), b_i \sim \mathcal{N}(0, 1)$ . Under this distributional assumption, it is easy to verify that  $\mathbb{E}_{a_i,b_i}[f_i(\mathbf{w})] = f(\mathbf{w})$ . As a result, the empirical objective is given as  $\hat{f} = \frac{1}{n} \sum_{i=1}^{n} f_i(\mathbf{w})$ , which is used in optimization. We set  $n = 64, \sigma = 0.1$  and  $\rho = 0.1$  for SAM and mSAM. The minimum of  $f(\mathbf{w})$  is  $(1 + \sigma^2)\sigma^2$  and is achieved as long as  $w_2 = 0$ . Indeed, we verify that GD and SAM converge to zero when run on f. Next, we run GD, SAM and mSAM on  $\hat{f}$  for 50,000 epochs, using the batch size of 32, and setting m = 4 for mSAM.

We record the largest eigenvalue of the Hessian of  $\hat{f}(\cdot)$ , as a measure of the sharpness of the solution over the course of the algorithm. This quantity for all epochs is shown in Figure 2. First, we note that mSAM follows a trajectory with a lower largest eigenvalue of the Hessian, implying the mSAM's trajectory is flatter. This observation corroborates our theoretical analyses and empirical findings. Interestingly, all methods used in this example converge to  $w_2 = 0$  and achieve the global minimum of  $\hat{f}$ . However, mSAM converges to a solution that is flatter.

### 4 Numerical Experiments

This section compares mSAM to SAM and vanilla optimization methods (i.e. without sharpness-aware modification) on various model architectures and datasets. We report the average and standard deviation of accuracy on the test data over five independent runs. We also note that we use the same values of hyper-parameters for all algorithms, where  $\rho$  is chosen based on the best validation performance for SAM, and other hyper-parameters are chosen based on the best validation error for vanilla methods. Moreover, although it is possible to use different values of  $\rho$  for each micro-batch in mSAM, doing so requires tuning numerous hyper-parameters, which is computationally infeasible. Therefore, we use the same value of  $\rho$  for all micro-batches.

Dataset Model Vanilla SAMмSAM  $96.40 \pm 0.06$ ResNet50 $95.45 \pm 0.10$  $96.09 \pm 0.11$ CIFAR 10 WRN-28-10  $95.92 \pm 0.12$  $96.95 \pm 0.04$  $96.90 \pm 0.05$ VIT-B/16  $97.68 \pm 0.03$  $97.75 \pm 0.06$  $98.29 \pm 0.08$ ResNet50  $80.68 \pm 0.13$  $81.49 \pm 0.18$  $83.37 \pm 0.10$ CIFAR 100 WRN-28-10  $81.01 \pm 0.19$  $82.93 \pm 0.13$  $84.07 \pm 0.06$ VIT-B/16  $88.02 \pm 0.17$  $88.75 \pm 0.07$  $89.00 \pm 0.17$ ResNet50  $76.35 \pm 0.09$  $76.61 \pm 0.07$  $76.79 \pm 0.09$ WRN50-2-BOTTLENECK  $79.36 \pm 0.04$  $78.04 \pm 0.09$  $78.50 \pm 0.09$ IMAGENET 1K ViT-S/32 $64.53 \pm 0.72$  $65.86 \pm 0.81$  $66.76 \pm 0.22$ 

Table 2: Accuracy Results for CNN Architectures

Table 3: Accuracy Results for GLUE Tasks

Task	Vanilla	SAM	mSAM (m=8)
COLA	$63.66 \pm 2.46$	$64.30 \pm 0.49$	$64.57 \pm 0.66$
MRPC SST-2	$89.79 \pm 0.05$ $94.27 \pm 0.18$	$90.37 \pm 0.13$ $95.21 \pm 0.12$	$90.92 \pm 0.16$ $95.38 \pm 0.10$
QQP	$91.70 \pm 0.11$	$92.13 \pm 0.02$	$92.18 \pm 0.03$

### 4.1 Image Classification

In our first set of experiments on image classification datasets, we compare the performance of mSAM, SAM and vanilla methods with multiple CNN architectures such as ResNets [2] and WideResNet [50]. We use CIFAR10/100 [51] and ImageNet [52] datasets as our test bed. We use different seeds for all five runs of each experiment.

The average accuracies corresponding to the experiments with the three datasets and the architectures of ResNet and WideResNet are reported in Table 2. For the CIFAR datasets, we use an effective batch size of 512 across four NVIDIA V100 GPUs. For the ImageNet dataset, we use an effective batch size of 2048 across eight GPUs. We use m=32 for mSAM for CIFAR and 4/8 for ResNet50 and WideResNet-50-2, respectively, for ImageNet. Details about hyper-parameters used to produce these results can be found in Appendix B. Overall, mSAM consistently leads to better accuracy than SAM and vanilla methods in all CNN-related experimental results reported in Table 2.

Following recent results that suggest that sharpness-aware optimization can substantially improve the generalization quality of Vision Transformers (ViTs) [29], we conduct additional experiments on ViT architectures. In particular, we use the pre-trained ViT-B/16 checkpoint from [53] and fine-tune the model

on CIFAR10/100 data independently. For ImageNet, we train a smaller version of the ViT model (ViT-S/32) from scratch. We choose 512 as the batch size for the CIFAR fine-tuning tasks and use 4096 as the batch size for training from scratch on the ImageNet dataset. The average accuracy results for ViT are reported in Table 2. Similar to results on CNNs, mSAM outperforms both SAM and vanilla training across all sets of ViT-related tasks. Note that we do not leverage any advanced data augmentation techniques, and only use inception-style image pre-processing. Other hyper-parameters to produce these results are listed in Appendix B.

### 4.2 NLP Fine-tuning

Our next set of experiments is based on four tasks from the GLUE benchmark [54]. In particular, we choose COLA and MRPC as two small datasets and SST-2 and QQP as two larger datasets for empirical evaluation. Fine-tuning experiments are performed with the RoBERTa-base model [6] on four NVIDIA V100 GPUs with an effective batch size of 32. For the ease of reproduction of the results, we tabulate all the hyper-parameters used in Appendix C. For the fine-tuning experiments, we report the average value of Matthews Correlation Coefficient for COLA, and average accuracy for other datasets in Table 3. Overall, mSAM performs better than the baseline methods on these datasets. However, the variance among different runs is comparably high for smaller datasets such as COLA and MRPC. On the other hand, the results on larger data such as SST-2 and QQP are expectedly more robust across different runs.

## 5 A Deeper Investigation of mSAM

To further understand the mSAM algorithm, we design and report some experiments in this section. Additional experimental results are moved to Appendix A.

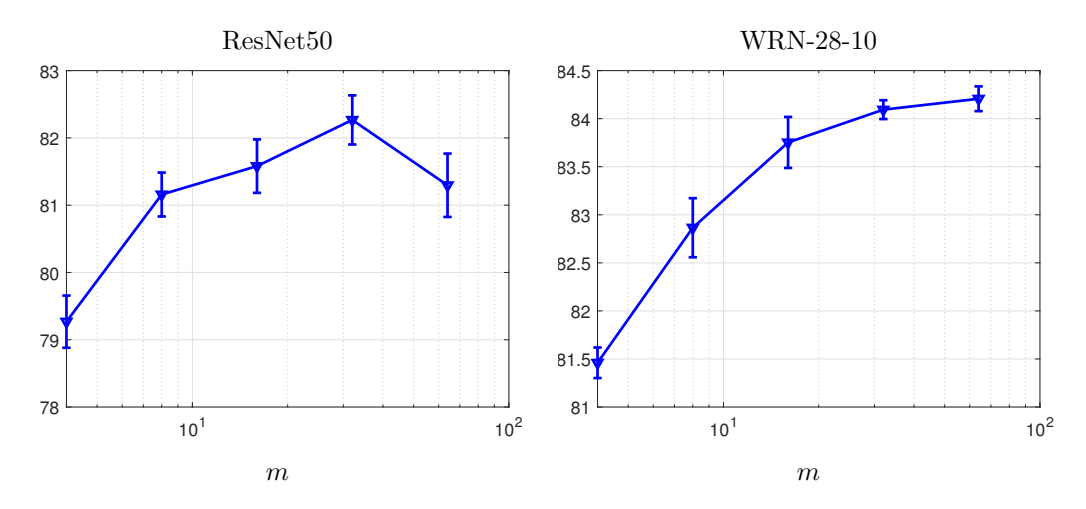


Figure 3: The effect of varying m on accuracy. We see that increasing m up to 32 results in better accuracy. However, increasing m further leads to worse results/marginal improvements.

Effect of varying m: In our experiments, we have observed that a larger value of m often leads to better test accuracy. We recover SAM by setting m=1, which produces inferior results. To test this hypothesis, we set up the experiments with the CIFAR100 dataset on two CNNs, ResNet50 and WRN-28-10, in the same setup as in Section 4.1. We run mSAM for different values of  $m \in \{4, 8, 16, 32, 64\}$ . The accuracy results for these experiments are shown in Figure 3.

Increasing m improves the performance up to  $m \approx 32$ . However, a value of m larger than this threshold either leads to worse performance or marginal improvements, so increasing m does not necessarily result in

better generalization. Intuitively, when the micro-batch is too small, the perturbation derived according to the micro-batch might not be a good estimate of the actual SAM perturbation, leading to worse performance. We leave the theoretical analysis of such a phenomenon an interesting direction for future research. We also note that understanding how the optimal value of m and batch size interact is an open question for future work.

Table 4:  $\lambda_{\text{max}}$  for CNNs

Model	Vanilla	SAM	мЅАМ
RESNET50 WRN-28-10	$26 \pm 2$ $92 \pm 4$	$\begin{array}{c} 21\pm 3 \\ 30\pm 2 \end{array}$	$\begin{array}{c} 18\pm1 \\ 17\pm1 \end{array}$

Are mSAM solutions flat? The SAM algorithm hypothesizes that flat solutions generalize better. Since mSAM consistently outperforms SAM, it is worth investigating if mSAM settles for even flatter solutions. To that end and to quantify sharpness, we calculate the largest eigenvalue of the Hessian of the loss function  $\mathcal{L}_{\mathcal{S}}(\mathbf{w})$  at the final solution, denoted as  $\lambda_{\text{max}}$ . This metric is widely accepted to be a good indicator of the sharpness/flatness of a solution [22]. We calculate  $\lambda_{\text{max}}$  over the full train data using power iteration, as implemented by [55]. We use the ResNet50 and WRN-28-10 models trained on CIFAR100 (see Section 4.1) to calculate  $\lambda_{\text{max}}$ . The average results for these experiments are reported in Table 4. We see that mSAM leads to solutions with smaller  $\lambda_{\text{max}}$  than SAM and vanilla SGD, which agrees with our theoretical results from Section 3.

mSAM runtime: A general misconception about mSAM is that it is computationally inefficient, as the total number of forward-backwards passes in the network is multiplied by m [30]. However, note that these passes are performed on micro-batches, which are m times smaller than the actual minibatch. Hence, the overall computational cost gets amortized and is never as high as m times the cost of SAM. In practice, on large networks, the runtime of mSAM is <u>only</u> 1.2-1.3 times more compared to SAM. In Appendix A, we present numerical evidence for mSAM efficiency and discuss a few hybrid algorithms to reduce the computational cost of mSAM even further.

### 6 Discussion

In this work, we provide theoretical justification that mSAM leads to even flatter solutions than SAM that extends a recent well-studied framework of stability dynamics. Intuitively, it is often the case that flatter minima lead to better generalization. The thorough empirical study that we also perform in the paper backs this theory and shows that mSAM outperforms SAM on different datasets (image classification and NLP tasks) and model architectures (CNNs and Transformers); the exact performance gap is primarily a function of the data and the architecture. Moreover, our experiments suggest that mSAM does not necessarily incur a substantially higher computational cost than SAM, making it amenable to large-scale problems. Our theoretical framework can be further generalized to splitting the mini-batch into micro-batches to improve flatness when the gradient computation is compositional, often seen in other variants of sharpness aware minimization. An exciting avenue for future work would be to further extend the flatness theory of splitting mini-batches into micro-batches for other gradient updates with non-linear aggregation. This technique could then be practically applied to other methods to improve generalization.

## Acknowledgements

Kayhan Behdin contributed to this work while he was an intern at LinkedIn during summer 2022. This work is not a part of his MIT research. Rahul Mazumder contributed to this work while he was a consultant for LinkedIn (in compliance with MIT's outside professional activities policies). This work is not a part of his MIT research.

### References

- [1] A. Krizhevsky, I. Sutskever, and G. E. Hinton. Imagenet classification with deep convolutional neural networks. Communications of the ACM, 60(6):84–90, 2017.
- [2] K. He, X. Zhang, S. Ren, and J. Sun. Deep residual learning for image recognition. In <u>Proceedings of the IEEE conference on computer vision and pattern recognition</u>, pages 770–778, 2016.
- [3] M. Tan and Q. Le. Efficientnet: Rethinking model scaling for convolutional neural networks. In International conference on machine learning, pages 6105–6114. PMLR, 2019.
- [4] A. Vaswani, N. Shazeer, N. Parmar, J. Uszkoreit, L. Jones, A. N. Gomez, Ł. Kaiser, and I. Polosukhin. Attention is all you need. Advances in neural information processing systems, 30, 2017.
- [5] J. Devlin, M. Chang, K. Lee, and K. Toutanova. Bert: Pre-training of deep bidirectional transformers for language understanding. arXiv preprint arXiv:1810.04805, 2018.
- [6] Y. Liu, M. Ott, N. Goyal, J. Du, M. Joshi, D. Chen, O. Levy, M. Lewis, L. Zettlemoyer, and V. Stoyanov. Roberta: A robustly optimized bert pretraining approach. arXiv preprint arXiv:1907.11692, 2019.
- [7] H. Guo, R. Tang, Y. Ye, Z. Li, and X. He. Deepfm: a factorization-machine based neural network for ctr prediction. arXiv preprint arXiv:1703.04247, 2017.
- [8] M. Naumov, D. Mudigere, H. Shi, J. Huang, N. Sundaraman, J. Park, X. Wang, U. Gupta, C. Wu, A. G. Azzolini, et al. Deep learning recommendation model for personalization and recommendation systems. arXiv preprint arXiv:1906.00091, 2019.
- [9] N. Keskar, D. Mudigere, J. Nocedal, M. Smelyanskiy, and P. Tang. On large-batch training for deep learning: Generalization gap and sharp minima. arXiv preprint arXiv:1609.04836, 2016.
- [10] S. Liu, D. Papailiopoulos, and D. Achlioptas. Bad global minima exist and sgd can reach them. <u>Advances</u> in Neural Information Processing Systems, 33:8543–8552, 2020.
- [11] I. Sutskever, J. Martens, G. Dahl, and G. Hinton. On the importance of initialization and momentum in deep learning. In International conference on machine learning, pages 1139–1147. PMLR, 2013.
- [12] D. P. Kingma and J. Ba. Adam: A method for stochastic optimization. <u>arXiv preprint arXiv:1412.6980</u>, 2014.
- [13] Y. You, J. Li, S. Reddi, J. Hseu, S. Kumar, S. Bhojanapalli, X. Song, J. Demmel, K. Keutzer, and C. Hsieh. Large batch optimization for deep learning: Training BERT in 76 minutes. arXiv preprint arXiv:1904.00962, 2019.
- [14] S. Jastrzebski, M. Szymczak, S. Fort, D. Arpit, J. Tabor, K. Cho\*, and K. Geras\*. The break-even point on optimization trajectories of deep neural networks. In <u>International Conference on Learning</u> Representations, 2020.
- [15] J. Cohen, S. Kaur, Y. Li, J.Z. Kolter, and A. Talwalkar. Gradient descent on neural networks typically occurs at the edge of stability. In <u>International Conference on Learning Representations</u>, 2021. URL https://openreview.net/forum?id=jh-rTtvkGeM.
- [16] G. K. Dziugaite and D. M. Roy. Computing nonvacuous generalization bounds for deep (stochastic) neural networks with many more parameters than training data. arXiv preprint arXiv:1703.11008, 2017.
- [17] Z. Xie, I. Sato, and M. Sugiyama. A diffusion theory for deep learning dynamics: Stochastic gradient descent exponentially favors flat minima. In <u>International Conference on Learning Representations</u>, 2021.

- [18] L. Wu, M. Wang, and W. Su. When does sgd favor flat minima? a quantitative characterization via linear stability, 2022. URL https://arxiv.org/abs/2207.02628.
- [19] J. Z. HaoChen, C. Wei, J. Lee, and T. Ma. Shape matters: Understanding the implicit bias of the noise covariance. In <u>Proceedings of Thirty Fourth Conference on Learning Theory</u>, volume 134, pages 2315–2357, 2021.
- [20] Samuel L. S. and Quoc V. L. A bayesian perspective on generalization and stochastic gradient descent. In International Conference on Learning Representations, 2018.
- [21] P. Foret, A. Kleiner, H. Mobahi, and B. Neyshabur. Sharpness-aware minimization for efficiently improving generalization. arXiv preprint arXiv:2010.01412, 2020.
- [22] L. Wu, C. Ma, and W. E. How sgd selects the global minima in over-parameterized learning: A dynamical stability perspective. In Advances in Neural Information Processing Systems, volume 31, 2018.
- [23] H. Ibayashi, T. Hamaguchi, and M. Imaizumi. Minimum sharpness: Scale-invariant parameter-robustness of neural networks. arXiv preprint arXiv:2106.12612, 2021.
- [24] J. Zhuang, B. Gong, L. Yuan, Y. Cui, H. Adam, N. Dvornek, S. Tatikonda, J. Duncan, and T. Liu. Surrogate gap minimization improves sharpness-aware training. arXiv preprint arXiv:2203.08065, 2022.
- [25] Y. Liu, S. Mai, X. Chen, C. Hsieh, and Y. You. Towards efficient and scalable sharpness-aware minimization. In Proceedings of the IEEE/CVF Conference on Computer Vision and Pattern Recognition, pages 12360–12370, 2022.
- [26] J. Du, D. Zhou, J. Feng, V. YF Tan, and J. T. Zhou. Sharpness-aware training for free. arXiv preprint arXiv:2205.14083, 2022.
- [27] J. Kwon, J. Kim, H. Park, and I. K. Choi. Asam: Adaptive sharpness-aware minimization for scale-invariant learning of deep neural networks. In Proc. of ICML, volume 139, pages 5905–5914, 2021.
- [28] M. Kim, D. Li, S. X. Hu, and T. M. Hospedales. Fisher sam: Information geometry and sharpness aware minimisation, 2022. URL https://arxiv.org/abs/2206.04920.
- [29] X. Chen, C. Hsieh, and B. Gong. When vision transformers outperform resnets without pre-training or strong data augmentations. arXiv preprint arXiv:2106.01548, 2021.
- [30] D. Bahri, H. Mobahi, and Y. Tay. Sharpness-aware minimization improves language model generalization. arXiv preprint arXiv:2110.08529, 2021.
- [31] M. Andriushchenko and N. Flammarion. Towards understanding sharpness-aware minimization. In International Conference on Machine Learning, pages 639–668. PMLR, 2022.
- [32] J. M. Cohen, B. Ghorbani, S. Krishnan, N. Agarwal, S. Medapati, M. Badura, D. Suo, D. Cardoze, Z. Nado, G. E. Dahl, and J. Gilmer. Adaptive gradient methods at the edge of stability, 2022. URL https://arxiv.org/abs/2207.14484.
- [33] S. Arora, Z. Li, and A. Panigrahi. Understanding gradient descent on edge of stability in deep learning, 2022. URL https://arxiv.org/abs/2205.09745.
- [34] P. L. Bartlett, P. M. Long, and O. Bousquet. The dynamics of sharpness-aware minimization: Bouncing across ravines and drifting towards wide minima, 2022. URL https://arxiv.org/abs/2210.01513.
- [35] K. Wen, T. Ma, and Z. Li. How does sharpness-aware minimization minimize sharpness?, 2022. URL https://arxiv.org/abs/2211.05729.

- [36] S. Ujváry, Z. Telek, A. Kerekes, A. Mészáros, and F. Huszár. Rethinking sharpness-aware minimization as variational inference, 2022. URL https://arxiv.org/abs/2210.10452.
- [37] C. Ma and L. Ying. On linear stability of SGD and input-smoothness of neural networks. In <u>Advances</u> in Neural Information Processing Systems, 2021.
- [38] J. Szücs, M. Levi, and V.I. Arnold. <u>Geometrical Methods in the Theory of Ordinary Differential Equations</u>. Grundlehren der mathematischen Wissenschaften. Springer New York, 2012. ISBN 9781461210375.
- [39] Z. Li, T. Wang, J. Lee, and S. Arora. Implicit bias of gradient descent on reparametrized models: On equivalence to mirror descent, 2022. URL https://arxiv.org/abs/2207.04036.
- [40] S. Gunasekar, J. Lee, D. Soudry, and N. Srebro. Characterizing implicit bias in terms of optimization geometry. In Proc. of ICML, pages 1832–1841, 2018.
- [41] Z. Li, S. Malladi, and S. Arora. On the validity of modeling sgd with stochastic differential equations (sdes). In Advances in Neural Information Processing Systems, volume 34, pages 12712–12725, 2021.
- [42] Y. Feng and Y. Tu. The inverse variance–flatness relation in stochastic gradient descent is critical for finding flat minima. Proceedings of the National Academy of Sciences, 118(9), 2021.
- [43] T. Mori, L. Ziyin, K. Liu, and M. Ueda. Logarithmic landscape and power-law escape rate of SGD, 2022. URL https://openreview.net/forum?id=rqolQhuq6Hs.
- [44] S. Wojtowytsch. Stochastic gradient descent with noise of machine learning type. Part II: Continuous time analysis. arXiv e-prints, page arXiv:2106.02588, June 2021. doi: 10.48550/arXiv.2106.02588.
- [45] J. Wu, W. Hu, H. Xiong, J. Huan, V. Braverman, and Z. Zhu. On the noisy gradient descent that generalizes as sgd, 2019. URL https://arxiv.org/abs/1906.07405.
- [46] R. Müller, S. Kornblith, and G. Hinton. When does label smoothing help?, 2019. URL https://arxiv.org/abs/1906.02629.
- [47] J. Geiping, M. Goldblum, P. E. Pope, M. Moeller, and T. Goldstein. Stochastic training is not necessary for generalization. CoRR, abs/2109.14119, 2021. URL https://arxiv.org/abs/2109.14119.
- [48] L. Dinh, R. Pascanu, S. Bengio, and Y. Bengio. Sharp minima can generalize for deep nets. <u>CoRR</u>. abs/1703.04933, 2017. URL http://arxiv.org/abs/1703.04933.
- [49] S. Kaur, J. Cohen, and Z. C. Lipton. On the maximum hessian eigenvalue and generalization, 2022. URL https://arxiv.org/abs/2206.10654.
- [50] S. Zagoruyko and N. Komodakis. Wide residual networks. arXiv preprint arXiv:1605.07146, 2016.
- [51] A. Krizhevsky, G. Hinton, et al. Learning multiple layers of features from tiny images. 2009.
- [52] O. Russakovsky, J. Deng, H. Su, J. Krause, S. Satheesh, S. Ma, Z. Huang, A. Karpathy, A. Khosla, M. Bernstein, A. C. Berg, and L. Fei-Fei. ImageNet Large Scale Visual Recognition Challenge. <u>International Journal of Computer Vision (IJCV)</u>, 115(3):211–252, 2015. doi: 10.1007/s11263-015-0816-y.
- [53] B. Wu, C. Xu, X. Dai, A. Wan, P. Zhang, Z. Yan, M. Tomizuka, J. Gonzalez, K. Keutzer, and P. Vajda. Visual transformers: Token-based image representation and processing for computer vision, 2020.
- [54] A. Wang, A. Singh, J. Michael, F. Hill, O. Levy, and S. Bowman. GLUE: A multi-task benchmark and analysis platform for natural language understanding. In <u>Proceedings of the 2018 EMNLP Workshop BlackboxNLP: Analyzing and Interpreting Neural Networks for NLP</u>, pages 353–355, Brussels, Belgium, November 2018. Association for Computational Linguistics.

[55] N. Golmant, Z. Yao, A. Gholami, M. Mahoney, and J. Gonzalez. pytorch-hessian-eigenthings: efficient pytorch hessian eigendecomposition, October 2018.

### A mSAM and Computational Efficiency

Since SAM requires two forward-backwards passes for each batch of data, SAM is almost twice as slow as vanilla training. In our experiments, mSAM appears to be slower than SAM, although not m times slower, as suggested by Bahri et al. [30]. To demonstrate that, we report the average runtime of our experiments from Section 4.1 on CIFAR100 data in Table A.1 and ImageNet data in Table A.2. Expectedly, SAM is almost twice as slow as the vanilla method in most cases (despite ViT-S/32 experiment where the common data pre-processing stage requires more time for preparing the images into a sequence of 32 patches). Interestingly, in the worst case, mSAM is <u>only</u> twice as slow as SAM, and in the best case, the computational penalty is only within 10% increase compared to SAM. The primary reason is that the overall computation complexity of forward-backwards passes for mSAM and SAM is not too different. In each epoch, mSAM performs m times more passes on micro-batches that are m times smaller.

Table A.1: Runtime of different methods and architectures on CIFAR100 data (in seconds)

Model	Vanilla	SAM	мЅАМ
RESNET50	$4497 \pm 11$	$7440 \pm 9$ $17483 \pm 40$ $7007 \pm 43$	$16196 \pm 77$
WRN	$10675 \pm 18$		$22261 \pm 24$
VIT-B/16	$4349 \pm 21$		$8163 \pm 14$

Table A.2: Runtime of different methods and architectures on ImageNet data (in hours)

Model	Vanilla	SAM	мЅАМ	
RESNET50 WRN-50-2-BOTTLENECK	$14.74 \pm 0.68 27.68 \pm 0.18$	$25.54 \pm 0.25$ $52.02 \pm 0.36$	$25.87 \pm 0.08$ $58.93 \pm 0.26$	
VIT-S/32	$19.91 \pm 0.13$	$24.50 \pm 0.26$	$30.66 \pm 0.2$	

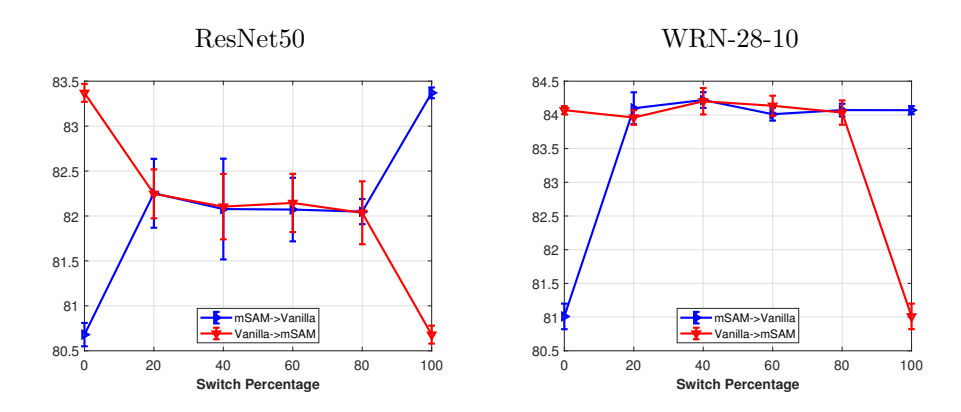


Figure A.1: Effect of switching training algorithm

Although mSAM does not appear to be computationally prohibitive in our experiments, it is still not as efficient as vanilla training, leaving room for further improving its efficiency. To that end, we conduct the following set of experiments. Building on our CIFAR100 experiments from Section 4.1, we start the training either with mSAM or vanilla training and then switch to the other training algorithm at some point. We keep all other training parameters fixed. The accuracy results for this setup for ResNet50 and WRN-28-10

Table B.1: Hyper-parameters for CIFAR10/100 experiments

Model	ResNet50	WRN-28-10	VIT-B/16 (FINE-TUNING)
Optimizer	SGD	SGD	AdamW
Peak Learning Rate	0.5	0.75	$10^{-3}$
Batch Size	512	512	512
Number of epochs	200	200	20
Momentum	0.9	0.9	-
Weight Decay	$5 \times 10^{-4}$	$5 \times 10^{-4}$	0.3
Label Smoothing	0.1	0.1	-
Learning Rate Schedule	ALL METH	HODS USE ONE C	YCLE WITH 5% WARM-UP
Gradient Clipping	-	-	NORM=1
$\rho \text{ (SAM/MSAM)}$	0.2	0.2	0.3
m  (MSAM)	32	32	32

Table B.2: Hyper-parameters for ImageNet experiments

Model	ResNet50	WRN-50-2-BOTTLENECK	ViT-S/32
Optimizer	SGD	SGD	AdamW
Peak Learning Rate	0.8	0.5	3E-3
Batch Size	2048	2048	4096
Number of epochs	90	100	300
Momentum	0.9	0.9	-
Weight Decay	$1 \times 10^{-4}$	$1 \times 10^{-4}$	0.3
Label Smoothing	0.1	0.1	-
Learning Rate Schedule	17.7% (5K STEP)	1%	10%
Gradient Clipping	-	-	NORM=1
$\rho \text{ (SAM/MSAM)}$	0.05	0.05	0.05
m  (MSAM)	4	8	8

are reported in Figure A.1. In this figure, the switch percent is the threshold in training when we transition from one algorithm to the other. For example, for the switch percent of 20, if we start with mSAM, we use mSAM for the first 20% of epochs and vanilla updates for the rest. If mSAM is used for the initial and/or final part of training, the accuracy is always better than vanilla training. In fact, in the WRN-28-10 case, as long as we partially use mSAM, the accuracy is almost the same as training with mSAM for the entire duration. For ResNet50, not using mSAM for the whole training leads to a drop in performance; however, even in this case, the accuracy of the hybrid training is better than the SAM training. These observations suggest that it is possible to enjoy the superior performance of mSAM, at least to some degree, while not having to deal with the computational complexity of mSAM for the entire training. A better theoretical and empirical understanding of the hybrid training method can be an exciting avenue for future work.

## B Hyper-parameters for Image Classification Experiments

As mentioned, our experiments on CIFAR data in this section are done on 4 Nvidia V100 GPUs, with an effective batch size of 512. For mSAM, we used the micro-batch size of 16, corresponding to m=32. The rest of the hyper-parameters are chosen as in Table B.1 for CIFAR10/100 experiments. For ImageNet experiments, we use 8 Nvidia V100 GPUs, with an effective batch size of 2048 for ResNet50 and WideResNet50-2-bottleneck, and 4096 for ViT-S/32. The micro-batch size and m are chosen based on a grid search within the set of  $\{2,4,8,16\}$ . The rest of the hyper-parameters are listed in Table B.2 for ImageNet experiments.

# C Hyper-parameters for GLUE Experiments

Table C.1: Hyper-parameters for NLP experiments

Task	COLA	MRPC	SST-2	QQP
Optimizer		A	DAMW	
Learning Rate	$10^{-5}$	$10^{-5}$	$5 \times 10^{-6}$	$2 \times 10^{-5}$
LEARNING RATE SCHEDULE	One cycle with 6% warm-up			
Number of Epochs	60	60	20	15
Weight Decay			0.01	
$\rho \; (SAM/MSAM)$	0.01	0.01	0.05	0.05

Our experiments in this section are done on four Nvidia V100 GPUs, with an effective batch size of 32. For mSAM, we have used the micro-batch size of four, which corresponds to m=8. The other hyper-parameters are listed in Table C.1.